Optimizing LUT-Based RTM Inversion for Semiautomatic Mapping of Crop Biophysical Parameters from Sentinel-2 and -3 Data: Role of Cost Functions

Jochem Verrelst, Juan Pablo Rivera, Ganna Leonenko, Luis Alonso, and José Moreno, *Member, IEEE*

***Abstract*—Inversion of radiative transfer models (RTM) using a lookup-table (LUT) approach against satellite reflectance data can lead to concurrent retrievals of biophysical parameters such as leaf chlorophyll content (Chl) and leaf area index (LAI), but optimization strategies are not consolidated yet. ESA's upcoming satellites Sentinel-2 (S2) and Sentinel-3 (S3) aim to ensure continuity of old generation satellite sensors by providing superspectral images of high spatial and temporal resolution. This unprecedented data availability leads to an urgent need for developing robust, accurate, and operational retrieval methods. For three simulated Sentinel settings (S2-10 m: 4 bands, S2-20 m: 8 bands and S3-OLCI: 19 bands) various optimization strategies in LUT-based RTM inversion have been evaluated, being the role of i) added noise, ii) multiple best solutions, iii) combined parameters ($Chl \times$ LAI), and iv) applied cost functions. By inverting the PROSAIL model and using data from the ESA-led field campaign SPARC (Barrax, Spain), it was demonstrated that introducing noise and opting for multiple best solutions in the inversion considerably improved retrievals. However, the widely used RMSE was not the best performing cost function. Three families of alternative cost functions were applied here: information measures, minimum contrast, and M-estimates. We found that so-called "Power divergence measure", "Trigonometric", and spectral measure with "Contrast function $K(x) = -\log(x) + x$", yielded more accurate results, although this also depended on the biophysical parameter. Particularly, when simultaneous retrieval of multiple biophysical parameters is the objective then "Contrast function $K(x) = -\log(x) + x$" provided most consistent optimized estimates of leaf Chl, LAI and canopy Chl across the different Sentinel configurations (relative RMSE: 24–29%).**

***Index Terms*—Automated radiative transfer models operator (ARTMO), chlorophyll content (Chl), leaf area index (LAI), lookup-table (LUT)-based inversion, PROSAIL, radiative transfer models (RTMs), Sentinel-2 (S2), Sentinel-3 (S3).**

Manuscript received May 2, 2012; revised October 19, 2012; accepted December 30, 2012. This paper was supported in part by the Spanish Ministry for Science and Innovation under projects: AYA2010-21432-C02-01 and CSD2007-00018. J. Verrelst was supported by the EU Marie Currie IEF Grant 252237.

J. Verrelst, J. P. Rivera, and L. Alonso are with the Image Processing Laboratory (IPL), Universitat de València. Paterna 46980, Spain (e-mail: jochem.verrelst@uv.es; juanri2@alumni.uv.es; luis.alonso@uv.es).

G. Leonenko is with Cardiff University, Wales CF10 3XQ, U.K. (e-mail: leonenkog1@cardiff.ac.uk).

J. Moreno is with the Department of Earth Physics and Thermodynamics, Faculty of Physics, University of Valencia, 46100 Burjassot, Spain (e-mail: jose.moreno@uv.es).

Color versions of one or more of the figures in this paper are available online at http://ieeexplore.ieee.org.

Digital Object Identifier 10.1109/TGRS.2013.2238242

I. Introduction

LEAF chlorophyll content (Chl) and green leaf area index (LAI) are among the most important biophysical parameters retrievable from optical Earth observation (EO) data [1], [2]. These parameters give insight in the phenological stage and health status (e.g., development, productivity, stress) of crops and forests. Chl can be considered as a bio-indicator of the plant's actual health status [3], [4], and of vegetation gross primary productivity [5]. Besides, LAI characterizes the structure and functioning of vegetation cover [6]. Because of its role as the interface between ecosystem and atmosphere and involvement in many processes, Chl and LAI are crucial in aboveground biomass estimation, vegetative evapotranspiration calculation, and the energy-exchange evaluation of terrestrial vegetation [7]–[10].

Currently, a multitude of EO data is available already, and this availability will increase enormously in the near future which will boost applications. The European Space Agency is now developing five new EO missions called Sentinels specifically for the operational needs of the "Global Monitoring for Environment and Security" (GMES) programme [11]. Five different Sentinel concepts have been planned. In particular, Sentinel-2 (S2) and Sentinel-3 (S3) are designed to provide continuity to monitoring services over global terrestrial surfaces by relying on superspectral (more than 10 and less than 50 bands, i.e., in-between multispectral and hyperspectral resolution) high spatial resolution (S2) and medium spatial resolution (S3) observations. Both Sentinel-2 and Sentinel-3 missions are based on a constellation of two satellites each to fulfil revisit and coverage requirements, providing robust data sets for GMES services. At the same time, further improvements of existing monitoring services from space are needed to better understand the environment dynamics at local and global scales. Therefore, along with these new missions, there is a demand of enhanced retrieval strategies of relevant biophysical parameters [12].

When it comes to the development of retrieval methods from EO data, it is mandatory to invest in methods that are both accurate and robust and at the same time can be applied in an operational context. Simple, yet widely accepted, empirical methods such as those based on vegetation indices, red-edge position, or spectral integral approaches work well under particular

sun-view geometry and for specific vegetation phenology, but they tend to produce inaccurate results when applied over a broad range of land cover types and optical and geometric conditions encountered in satellite images [13], [14]. Canopy reflectance, after all, is the result of several intricately coupled physical processes (i.e., canopy characteristics, soil background effects, sun-view geometry), which makes it difficult to estimate the influence of a single biophysical parameter from experimental data [15].

Contrary to empirical approaches, canopy radiative transfer models (RTMs) explicitly interpret driving processes between solar radiation and the elements constituting the canopy using physical laws. From a radiative transfer point of view, a vegetation canopy can be considered as an ensemble of scattering elements, bounded by the background vegetation and soil [16]. In these RTMs, top-of-canopy (TOC) reflectance is a function of canopy structural variables such as LAI, sun and viewing geometry, optical leaf and soil properties. In the same way, leaf optical properties can be described by a leaf RTM, i.e., as a function of leaf structure and biochemical parameters such as Chl. When a leaf RTM is coupled with a canopy RTM then leaf biochemical and canopy biophysical parameters (e.g. Chl and LAI) can be simultaneously retrieved through model inversion [17].

Because of being physically based, inversion of canopy RTMs against actual EO data is generally considered as one of the most accurate approaches to map biophysical parameters [18], [19]. However, this approach is not straightforward. According to Hadamarad postulates, mathematical models of physical phenomena are mathematically invertible if the solution of the inverse problem to be solved exists, is unique and depends continuously on variables [20]. Unfortunately this assumption is not met. In fact, the inversion of canopy RTMs is by nature an ill-posed problem mainly for two reasons [21]: On the one hand, several combinations of canopy biophysical and leaf biochemical parameters have a mutually compensating effect on canopy reflectance thus leading to very similar solutions. On the other hand, model uncertainties and simplifications (e.g., 1-D nature of some models) may induce large inaccuracies in the modeled canopy reflectance [22].

Over the past two decades, different successful strategies have been proposed to reduce the drawback of ill-posedness, including Lookup-table (LUT)-based inversion strategies [19], [20], [23]–[26], hybrid approaches in which LUTs are generated to feed machine learning approaches such as artificial neural network methods [27]–[30], Bayesian systems [31] and support vector regression [21], or LUT-based iterative numerical optimization methods [32]. The main advantage of LUT-based inversion approaches is that it can be fast because the most computationally expensive part of the inversion procedure is completed before the inversion itself.

LUT-based inversion in its essential form, i.e., direct comparison of LUT spectra against an observed spectra through a cost function (also in some cases known as distance, merit function, metric or divergence measure), constitutes the majority of applied inversion approaches. Various regularization strategies have been proposed to increase the robustness of the estimates: 1) the use of prior knowledge about model parameters [19], [23], [33]–[35], 2) the use of multiple best solutions (instead of the single best solution) [24], [33], [36], [37], 3) adding noise to account for uncertainties attached to measurements and models [24], [36], [37], and, 4) the combination of single variables into synthetic variables such as the canopy level content of absorbing materials [18], [25], [29], [38], e.g., canopy Chl, which is the product of leaf Chl and LAI.

Nevertheless, in view of applying these regularization strategies into a more operational context, aforementioned studies are constrained in various ways. First, while the majority of reviewed studies focused on optimizing a single LUT-based inversion problem, the mutual impact of proposed optimizing strategies has not been systematically assessed. Second, in most of these studies the well-known root mean square error (RMSE) was used as cost function between simulated and measured spectra. However, in case of outliers and nonlinearity, the residuals are distorted and therefore the key assumption for using RMSE (Gaussian or zero mean white noise distribution of residuals) is violated [39]. The latter authors suggested that alternative cost functions may provide a more robust way to estimate biophysical parameters since they allow retrievals for cases where errors are not normally distributed and allow to deal with nonlinear high parametric problems. The availability of a large number of cost functions gives a high degree of flexibility, since it allows model optimization for a wide range of error distributions. Hence, alternative cost functions deserve to be evaluated in view of the above-described optimizing strategies. Third, the majority of these studies focus on a specific vegetation type such as crop types, identified within the image [24], [37], [40]. This assumes that up-to-date knowledge of land cover types is available, which is usually not the case in an operational context. Moreover, eventually LUT-based inversion should be applicable not only for agroecosystems but over all natural and semi-natural vegetated surfaces. And fourth, from a practical perspective, hardly any of aforementioned studies provide links to software packages where proposed optimization strategies have been implemented.

In this paper, we aim to systematically evaluate different LUT-based inversion strategies in view of forthcoming Sentinel-2 and Sentinel-3 data streams for the benefit of improved pixel-wise estimation of biophysical parameters. The mutual impact of the following strategies were investigated: 1) the role of number of bands (e.g., different Sentinel band settings), 2) the role of added noise, 3) the role of multiple best solutions, 4) the role of combined variables, and finally: 5) the role of applied cost functions in these strategies. Data used came from the ESA-led field campaign SPARC, http://www.uv.es/leo/sparc/, which took place on the agricultural test site Barrax, Spain.

The remainder of the paper is organized as follows. Section II revises state-of-the-art semiautomatic LUT-based inversion approaches and briefly describes the developed toolbox ARTMO. Section III outlines different families of cost functions, briefly describes the data set used, the Sentinel-2 and -3 imagery and generated LUTs. Section IV shows the numerical results and final maps. Section V discusses main findings and Section VI concludes the paper.

II. State-of-the-Art Automated LUT-Based Inversion

Despite that numerous LUT-based inversion strategies have been proposed, only a few of these approaches have been implemented into a software package to enable semiautomatic mapping of biophysical parameters. One example is CRASh (Canopy variable Retrieval Approach based on PROSPECT and SAILh), designed for the concurrent retrieval of biophysical parameters from high-resolution EO data [35]. A similar toolbox was developed by [41], called REGLEX (REGularized canopy reFLECtance). This modeling tool couples leaf optics (PROSPECT), canopy reflectance (ACRM), and atmospheric radiative transfer (6SV1) model components, facilitating the direct use of at-sensor radiances in green, red and near-infrared wavelengths for the inverse retrieval of leaf Chl and LAI. An attractive feature of these toolboxes is that the inversion can be set class-based, thereby making use of LUT configurations per land cover class (e.g., agricultural fields). A drawback is that in each of these approaches only one leaf or canopy model can be chosen. In reality, however, a variety of RT models exists, each of them with specific characteristics, e.g., 1-D models for interpretation of homogeneous vegetated land covers and 3-D models for interpretation of heterogeneous vegetated land covers. In an attempt filling up this gap, we have recently developed an alternative toolbox, ARTMO (Automated Radiative Transfer Models Operator) [42], [43], in which the user can choose from multiple leaf and canopy RT models to generate class-based LUTs.

ARTMO is a GUI toolbox written in Matlab. This innovative toolbox provides essential tools for running and inverting a suite of plant reflectance models. In short, the toolbox enables the user: i) to choose between various plant leaf (e.g., PROSPECT-4, PROSPECT-5) and canopy reflectance models (e.g., 4SAIL, SLC, FLIGHT), ii) to choose between spectral band settings of various air- and space-borne sensors or defining new sensor band settings, iii) to simulate a massive amount of spectra and storing them in a relational database, iv) to evaluate LUT-based model inversion strategies against validation data given selected cost functions, optimization options and accuracy estimates and apply then a selected strategy to an EO image. Moreover, ARTMO is able to run inversions per land cover class, which permits realistic retrievals of biophysical parameters over patchy landscapes. For instance, agricultural fields can be interpreted by a 1-D model while forests can be interpreted by a 3-D model. Here, ARTMO has been used for evaluation LUT-based inversion over an agroecosystem that spans various crop types.

III. Methodology

A. Cost Functions

Numerical solution of the inverse problem adjusts the model parameters such that model predicted values closely match the measured values. The match between model output and data is usually based on minimizing the sum of least squares, as in RMSE. Another way to obtain better estimates is using alternative cost functions, e.g., as those introduced in [39]. The latter authors investigated several families of cost functions on simulated reflectance data for conifer and broadleaf cover. In general, statistical distances can be categorized into three families: *information measures*, *minimum contrast*, and *M-estimates*. Although they all represent "distance" or "metric" between two functions the main difference of these families is the way how reflectance functions are interpreted and in what space. These metric families came from different areas of mathematics and statistics and play an important role in image processing, engineering, medicine and code theory. They allow to take into the account nonlinearity of the problem, robustness and skewness of the noise to provide better retrievals of biophysical parameters. Moreover, contrary to using one cost function, the availability of a large number of statistical distances or divergence measures gives a high degree of flexibility, since it allows model optimization for different assumptions on the nature and properties of errors [39].

Based on the research in [39] we initially compared all the available cost functions (62) and selected three cost functions from the different families which may provide promising results as alternative to RSME. Let $D[P,Q]$ represent a distance between two functions, where $P=(p(\lambda_1),\ldots,p(\lambda_n))$ is satellite and $Q=(q(\lambda_1),\ldots,q(\lambda_n))$ is LUT correspondent reflectances and $\lambda_1,\ldots,\lambda_n$ represent n bands.

First cost function belongs to the family of *information measures*. This class represents different distances between two probability distributions and were widely explored throughout mathematical applications, see [44]. In this case we consider reflectance as probability distribution function and normalization is required (sum of probabilities is 1) prior to numerical application. Within this family, the "Power divergence measure" was introduced in [45] and it has the following form:

$$D[P,Q]=\sum_{\lambda_i=1}^{\lambda_n} p(\lambda_i)\frac{\{[p(\lambda_i)/q(\lambda_i)]^{\alpha}-1\}}{\alpha(\alpha+1)}, \alpha\in(-\infty,+\infty). \tag{1}$$

Note that in some cases for parameter $\alpha=-2,-1,-1/2,0,1$ we can get the following already known measures: the Neyman chi-squared measure divided by 2, the Kullback–Leibler divergence, the twice-squared Hellinger distance, the likelihood disparity, and the Pearson's chi-squared divided by 2. More information about all the above measures can be found in [44].

Second cost function belongs to the family of *M-estimates* which are a broad class of estimators that are obtained as the minima of sums of functions of the data. Least-squares estimators and many maximum-likelihood estimators are M-estimators. They are obtained by replacing square loss function into another more general convex function, see [46]. In this case we interpret reflectance as nonlinear regression function. One of the well-known distances from this class is RMSE which, for Gaussian error distributions, is consistent, asymptotically normal and asymptotically efficient. However, when the error distribution is non-Gaussian or nonsymmetric, the RMSE can result in large losses of efficiency. Thus, for RMSE the function can be represented in the following form:

$$D[P,Q]=\sqrt{\frac{\sum_{\lambda_i=1}^{\lambda_n}\left(p(\lambda_i)-q(\lambda_i)\right)^2}{n}}. \tag{2}$$

An alternative function with parameters $\alpha, \beta > 0$, is the so-called "trigonometric" distance, which is defined as

$$D[P,Q] = \sum_{\lambda_i=1}^{\lambda_n} \alpha x(\lambda_i) \arctan\left(\beta * x(\lambda_i)\right) - \alpha \frac{\log\left(\beta^2 \left(x(\lambda_i)\right)^2 + 1\right)}{2\beta} \quad (3)$$

where $x(\lambda_i) = p(\lambda_i) - q(\lambda_i)$. It is known that errors in this case are distributed by a logistic distribution. The parameters α, β provide better flexibility to match the cost function to the error distribution. The user needs to identify them by statistical learning. As it was mentioned above, M-estimates (those which differ from RMSE) corresponds to the maximum likelihood estimator of non-Gaussian errors (chi-square, gamma, etc). It means, for example in (3), that if the cost function provides better biophysical parameter estimation the errors have logistic distribution. Other distances can be also reinterpreted in form of the distributions of errors. Thus, identifying the best performing cost function and identifying the parameters is nothing else then estimation of observation errors.

The third cost function belongs to the family of *minimum contrast estimates*, where we consider reflectance as a spectral density function of some stochastic process. The basic idea behind it is to minimize the distance (contrast) between a parametric model and a nonparametric spectral density. Since one can interpret satellite observations as measurements in the spectral domain these distances seem to be a natural choice for analyzing satellite data. We consider the following spectral distance with the so-called "Contrast function $K(x) = -log(x) + x$", which were introduced in [47], [48], then distance has the form

$$D[P,Q] = \sum_{\lambda_i}^{\lambda_n} \left\{ -\log\left(\frac{q(\lambda_i)}{p(\lambda_i)}\right) + \frac{q(\lambda_i)}{p(\lambda_i)} \right\}. \quad (4)$$

More information about these and other cost functions can be found in [39].

B. SPARC Database

Ideally, LUT-based inversion strategies should be validated by a data set that represents the same variety of actual crops and conditions as remotely observed by the optical sensor. A diverse field data set, covering various crop types, growing phases, canopy geometries and soil conditions was collected during SPARC (SPectra bARrax Campaign). The SPARC-2003 and SPARC-2004 campaigns took place in Barrax, La Mancha, Spain (coordinates $30^\circ 3'$N, $28^\circ 6'$W, 700 m altitude). The test area has an extent of 5 km $\times$ 10 km, and is characterized by a flat morphology and large, uniform land-use units. The region consists of approximately 65% dry land and 35% irrigated land. The annual rainfall average is about 400 mm.

In the 2003 campaign (12–14 July) biophysical parameters were measured within a total of 113 Elementary Sampling Units (ESU) among different crops. ESU refers to a plot size of about 20^2 m^2. The same field data were collected in the 2004 campaign (15–16 July) within a total of 18 ESUs among different crops. Leaf Chl was derived by measuring within each ESU about 50 samples with a calibrated CCM-200 Chlorophyll Content Meter [49]. Green LAI was derived from canopy measurements made with a LiCor LAI-2000 digital analyzer. Each ESU was assigned to a LAI value, which was obtained as a statistical mean of 24 measures (8 data readings $\times$ 3 replications) with standard errors between 5 and 10% [50]. Contrary to earlier studies [51], [52], no bare soil samples were added in the validation data set because inversion of canopy RTMs is only relevant over vegetated land covers.

For both years, we have a total of 9 crops (garlic, alfalfa, onion, sunflower, corn, potato, sugar beet, vineyard and wheat), with field-measured values of LAI that vary between 0.4 and 5.9 (μ: 3.0, SD: 1.5) and Chl between 10 and 52 (μ: 38, SD: 14) μg/cm^2. Further details on the measurements can be found in [53], [54].

C. Sentinel-2 and -3 Configurations

1) Sentinel-2: The upcoming Sentinel-2 (S2) satellites capitalizes on the technology and the vast experience acquired with SPOT and Landsat over the past decades. S2 will be a polar-orbiting, superspectral high-resolution imaging mission [55]. The mission is envisaged to fly a pair of satellites with the first planned to launch in 2013. Each S2 satellite carries a Multi-Spectral Imager (MSI) with a swath of 290 km. It provides a versatile set of 13 spectral bands spanning from the visible and near infrared (VNIR) to the shortwave infrared (SWIR), featuring four bands at 10 m, six bands at 20 m and three bands at 60 m spatial resolution comparable to Landsat and SPOT. S2 incorporates three new bands in the red-edge region, which are centered at 705, 740 and 783 nm. The pair of S2 satellites aims to deliver data taken over all land surfaces and coastal zones every five days under cloud-free conditions, and typically every 15–30 days considering the presence of clouds [56]. To serve the objectives of GMES, S2 satellites will provide imagery for the generation of high-level operational products (level 2b/3) such as land-cover and land-change detection maps and geophysical variables such as Chl, LAI and leaf water content maps. To ensure that the final product can meet the user requirements, the GMES user committee defined an accuracy goal of the biophyical products of 10% [56].

2) Sentinel-3: The pair of Sentinel-3 (S3) satellites will provide global, frequent and near real-time ocean, ice and land monitoring. It continues Envisat's altimetry, the superspectral, medium-resolution VNIR ocean and land-surface observations of ERS, Envisat and SPOT-Vegetation, and includes enhancements to meet the operational revisit requirements and to facilitate new products and evolution of services. S3 will be equipped with the Ocean and Land Colour Instrument (OLCI), which will provide continuity of the existing MERIS mission. Six new bands have been added upon recommendations to improve the existing MERIS atmospheric and aerosol correction capabilities [57]. The OLCI ground resolution requirement depends whether the data are acquired above open ocean, or coastal zones and land. OLCI products provide a spatial

TABLE I
TESTED SENTINEL CONFIGURATIONS

Sentinel	S2-10m	S2-20m	S3-300m
Spatial resolution [m]	10	20	300
# bands	4	8 (4 + 4 at $<$ 20 m)	19
Band position	B2, B3, B4 and B8	B2 to B8a	O2 to O20
Wavelengths [nm]	490-665 and 842	490-865	413-940

resolution at sub-satellite point of 1200 m over open ocean and sea ice, and 300 m over coastal zones, while land products provide a resolution of 300 m globally. OLCI aims to be optimized to measure the ocean color over the open ocean and coastal zones, however, in such a way that it will not saturate over land targets. Its spectral bands are in the VNIR spectral range (from 403 to 1040 nm) with bandwidths ranging from 3.75 to 40 nm.

3) Simulated Sentinel-2 and -3 Imagery: S2 MSI and S3 OLCI imagery were simulated on the basis of Compact High-Resolution Imaging Spectrometry (CHRIS) data. CHRIS provides high spatial resolution hyperspectral data over the VNIR spectra from 400 to 1050 nm. It can operate in different modes, balancing the number of spectral bands, site of the covered area and spatial resolution because of on-board memory storage reasons [58]. We made use of nominal nadir CHRIS observations in Mode 1 (62 bands, maximal spectral information), which were acquired during the SPARC campaign. CHRIS Mode 1 has a spatial resolution of 34 m at nadir. The spectral resolution provides a bandwidth from 5.6 to 33 nm depending on the wavelength. The images were geometrically corrected [59], followed by atmospheric correction according to the method proposed in [60]. The nadir image from 12 July 2003 was used for spectral and spatial resampling to the settings of S2 and S3. Because featuring bands with different pixel sizes (10, 20 and 60 m), it is of special interest simulating S2 configurations both as a function of band settings and pixel size. Nearest neighbor was used for the spatial resampling and a Gaussian model with FWHM spacings was used for spectral resampling. Constrained by the spectral range of CHRIS, the following three Sentinel settings were generated, "S2-10 m": four bands at 10 m, "S2-20 m": eight bands at 20 m (4 bands at 20 m plus the S2-10 m bands coarse-grained at 20 m), and "S3-300 m": S3 OLCI configuration coarse-grained at 300 m. An overview of these configurations is provided in Table I. Note that we did not consider the S2 bands at 60 m because of being atmospheric bands. These bands are intended for atmospheric applications, such as aerosols correction, water vapor correction and cirrus detection [56] and are unable to deliver TOC reflectances that are interpretable by canopy RT models.

D. LUT Generation

From the available models in ARTMO we chose to couple PROSPECT-4 with 4SAIL because of being fast, invertible and well-representing homogeneous plant covers on flat surfaces areas such as those present at Barrax. Both models, hereafter referred as PROSAIL, have been used extensively over the past few years for a variety of applications (for a review see [17]). PROSPECT-4 calculates leaf reflectance and transmittance over the solar spectrum from 400 to 2500 nm at a 1 nm spectral sampling interval as a function of its biochemistry and anatomical structure. It consists of 4 parameters, being leaf structure, chlorophyll content (Chl), equivalent water thickness and dry matter content [61]. 4SAIL calculates top-of-canopy reflectance. 4SAIL inputs consist of: LAI, leaf angle distribution, ratio diffuse/direct irradiation, a hot spot parameter and sun-target-sensor geometry. Spectral input consists of leaf reflectance and transmittance spectra, here coming from PROSPECT-4, and a a moist and dry soil reflectance spectrum [62]. To obtain these soil spectra, the average of bare soil signature was calculated from bare moist and dry soil pixels identified in the imagery. In 4SAIL a scaling factor, α_{soil}, has been introduced that takes variation in soil brightness into account as a function of these two soil types.

TABLE II
RANGE AND DISTRIBUTION OF INPUT PARAMETERS USED TO ESTABLISH THE SYNTHETIC CANOPY REFLECTANCE DATABASE FOR USE IN THE LUT

	Model Parameters	Units	Range	Distribution
Leaf parameters: PROSPECT-4				
N	Leaf structure index	unitless	1.3-2.5	Uniform
Chl	Leaf chlorophyll content	[μg/cm^2]	5-75	Gaussian (μ: 35, SD: 30)
C_m	Leaf dry matter content	[g/cm^2]	0.001-0.03	Uniform
C_w	Leaf water content	cm	0.002-0.05	Uniform
Canopy variables: 4SAIL				
LAI	Leaf area index	[m^2/m^2]	0.1-7	Gaussian (μ: 3, SD: 2)
ALA	Average leaf angle	[°]	40-70	Uniform
α_{soil}	Soil scaling factor	unitless	0-1	Uniform
HotS	Hot spot parameter	[m/m]	0.05-0.5	Uniform
skyl	Diffuse incoming solar radiation	[fraction]	0.05	-
θ_s	Sun zenith angle	[°]	22.3	-
θ_v	View zenith angle	[°]	20.19	-
ϕ	Sun-sensor azimuth angle	[°]	0	-

The bounds and distributions of the PROSAIL variables are depicted in Table II. Variable bounds were taken from measurement campaigns and/or other studies working with the same crops [24], [37]. They were chosen to describe the characteristics of all crop types used in the study. Gaussian input distributions were generated for LAI and leaf Chl content to put more emphasis on the variable values being present in the actual growth stages of the crops. Sun and viewing conditions correspond to the situation of the satellite overpass.

ARTMO produced simulations for all possible combinations of the selected leaf and canopy input values, detailed in Table II. A LUT size of 100 000 TOC reflectance realizations was subsequently randomly chosen according to [25], [37]. This number was recently confirmed by [38], who concluded that a larger LUT size may not influence the estimation accuracy of state parameters much. All input parameters, metadata and associated output simulations were automatically stored in a relational database running underneath ARTMO. In this paper, no use was made of ARTMO's class-based inversion options because it was assumed that in an operational context no prior land cover information is available.

Two regularization options are commonly applied in LUT-based inversion strategies. First, often a Gaussian (white) noise is added to the simulated canopy reflectance [29], [63]. Different numbers are encountered in literature, typically spanning from 2.5 to 20% [23], [36], [37], meaning that this strategy is

not consolidated yet. To clarify its role in LUT-based inversion, a systematic assessment is pursued here, ranging from 0 (no noise) until 30% noise. Second, several studies demonstrated that the single best parameter combination corresponding to the smallest RMSE does not necessarily lead to best accuracies [19], [33]. A widely applied strategy is therefore taking the mean of multiple best solutions. Also, here different numbers are encountered in literature, spanning from the single best solution to the mean of the 20% best solutions [26], [36], [37]. Although recently [38] assessed the impact of this optimization strategy over a range of multiple solutions, its role in view of different noise levels and cost functions remains to be evaluated. Therefore, a range from 0 (single best solution) to the mean of 30% best solutions has been included in the analysis.

Thus, to summarize, we have:

- Relevant biophysical parameters: Chl, LAI and canopy $Chl (Chl \times \text{LAI})$.
- Three different Sentinel configurations with different band settings: S2-10 m (4 bands), S2-20 m (8 bands) and S3-300 m (19 bands).
- Addition of Gaussian noise on simulated spectra: 0–30%.
- Use of multiple sorted best solutions in the inversion: 0–30%.
- Four different cost functions: RMSE, "Power divergence measure", "Logistic distribution Trigonometric" and "Contrast function $K(x) = -\log(x) + x$". Data normalization was applied to the first two functions.

Given all these factors, their effects on the robustness of LUT-based inversion has been assessed. The retrieved predictions were compared against the measured validation data set using the normalized or relative RMSE (RRMSE), which is calculated by dividing the RMSE with the mean of the sample set. Additional statistics are also provided (RMSE, coefficient of determination (r^2)).

IV. Numerical Results

A. RMSE Cost Functions

The commonly used cost function RMSE (2) was first evaluated. The retrieved biophysical parameters were subsequently validated against the validation data set using the relative RMSE (RRMSE); further referred as relative error to avoid confusion with RMSE as cost function. Fig. 1 shows relative error matrices displaying the impact of noise levels against multiple best solutions in the inversion process for simulated S2-10 m, S2-20 m and S3-300 m data for leaf Chl, LAI and canopy $Chl (Chl \times \text{LAI})$. Best realized result per matrix are shown in Table III. Several observations can be made from these matrices.

First, opting for the very single best solution (see left-bottom corner in relative error matrices) appeared to be a poor inversion strategy in all scenarios (parameter and Sentinel band setting), especially when noise is introduced (see the bottom line in the matrices). Inversion clearly benefited from regularization strategies as compared to without them. Specifically LAI and canopy Chl retrievals gained from regularization options. For instance, relative errors improved from 190% (no regularizations) to 41% (for 1% multiple solutions, 22% noise) for LAI S2-20. Although for leaf Chl the added value of these regularization options was less extreme, they still fully proved its use. For S2-20 m, relative errors improved from 42% (no regularizations) to 20% (for 20% multiple solutions, 10% noise), and the same order of magnitude was encountered along the other Sentinel configurations.

Second, the obtained relative error matrices revealed that the tested biophysical parameters respond very differently to the regularization options. On the one hand, leaf Chl appeared to be a robust retrievable parameter for all band settings once having some best solutions and noise introduced. Variations in regularizations hardly impacted retrievals, only at high noise levels (e.g., $> 20\%$) accuracies started to degrade. On the other hand, LAI responded far more unstable than Chl and regularization options played an important role in improving its retrievals. In fact, the introduction of even low levels of noise and multiple solutions still led to failure of LAI retrievals. Only when injecting high noise levels more or less acceptable relative error results of about 40% were obtained. Note hereby that leaf Chl was less optimally retrieved in this region. Hence, given observed differences in leaf Chl and LAI behavior, it is not recommended to opt for implementing the same regularization

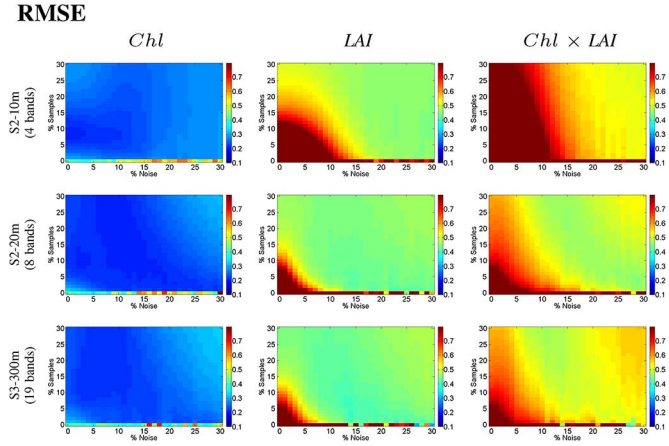

Fig. 1. Relative RMSE (RRMSE) matrices (×100%) using RMSE as cost function displaying the impact of % noise (X-axis) against multiple solutions (Y-axis) in LUT-based RTM inversion for S2-10 m (top), S2-20 m (middle) and S3-30 0 m (bottom) data for leaf Chl (left), LAI (middle) and canopy Chl (right). The more bluish, the better the estimate.

TABLE III
Statistics (r^2, RMSE, RRMSE) Based on Best Evaluated RRMSE and Corresponding Mean Multiple Solutions (%) and Noise Level (%) Using RMSE as Cost Function

Parameter	r^2	abs. RMSE	RRMSE	mult. sol. (%)	noise (%)
RMSE					
S2-10m:					
Chl	0.68	8.22	20.22	8	0
LAI	0.68	1.20	44.28	3	28
$Chl \times$ LAI	0.68	58.86	50.65	30	30
S2-20m:					
Chl	0.73	7.42	20.12	20	10
LAI	0.62	1.13	40.75	1	22
$Chl \times$ LAI	0.75	50.36	45.38	4	29
S3-300m:					
Chl	0.66	7.91	21.02	13	4
LAI	0.62	1.06	30.42	0	27
$Chl \times$ LAI	0.72	64.48	40.4	0	27

strategy to all retrievable parameters when using cost function RMSE.

Third, the relative error matrices also reveal that the number of bands play a role in the inversion. Especially LAI and canopy Chl retrievals benefited from having more bands included. For LAI, best matrix results improved from 44.3% (S2-10 m; 4 bands) to 30.4% (S3-300 m; 19 bands) (Table III). In this respect, the 4 bands of S2-10 m seems to be suboptimally configured to deliver robust LAI estimation.

A final observation is that the product of Chl and LAI (canopy Chl), as sometimes suggested to bypass the ill-posed problem (e.g., [33]), did not lead to superior results when using RMSE as cost function. Rather the contrary occurred; retrieval performances degraded significantly compared to their individual parameters. Adding noise somewhat improved accuracies, but they never went below a relative error of 40% (see also Table III).

B. Alternative Cost Functions

Apart from the typically applied regularization options, an attractive strategy to further improve retrieval performances would be to implement alternative cost functions. In continuation of the work of [39], the following alternative cost functions were evaluated, being "Power divergence measure", "Trigonometric" and spectral cost function with "Contrast function $K(x) = -\log(x) + x$". The same kind of relative error matrices as before were computed and are shown in Fig. 2. Associated best obtained results per relative error matrix are shown in Table IV.

First, the "Power divergence measure" (1) was found to be promising because it was the only cost function that outperformed RMSE in Chl estimation in all Sentinel scenarios, with relative error improvements of about 1–2%. It also led to more robust performances across the matrices than RMSE and also LAI and canopy Chl were considerably better retrieved. Best LAI performances improved up to 15% compared to RMSE. For canopy Chl relative errors lowered even about 14–27% (see Table IV). However, failures still occurred in case of S2-10 m at low multiple solutions and noise levels. It is also important to note that in this function a value to parameter α needs to be given, which provides more flexibility for better parameter estimation. To find the best parameter for the cost function we use simple statistical learning of testing them all on the grid from 0 to 200 with step of 20. The best cost function parameter is defined as minimum from all the retrieved biophysical parameter on the grid. The α parameter was for most of the scenarios optimized at 20.

Second, "Trigonometric" cost function (3) yielded robust leaf Chl retrievals across the relative error matrices. Best results were overall slightly poorer than RMSE (on the order of 1–3% RRMSE), notwithstanding this algorithm yielded on the whole better LAI and canopy Chl retrievals accros the matrices than aforementioned functions. Even better LAI accuracies than leaf Chl were achieved for S2-20 m and S3-300 m (see Table IV), though the matrices also show that accuracies degraded with high noise levels (e.g., $> 20\%$). For "Trigonometric" two parameters (α, β) need to be fine-tuned. For both of these parameters the same numeric array as "Power divergence measure" was applied. It was found that this function performed more or less similar over all scenarios, with α typically optimized at 20 and β at 180.

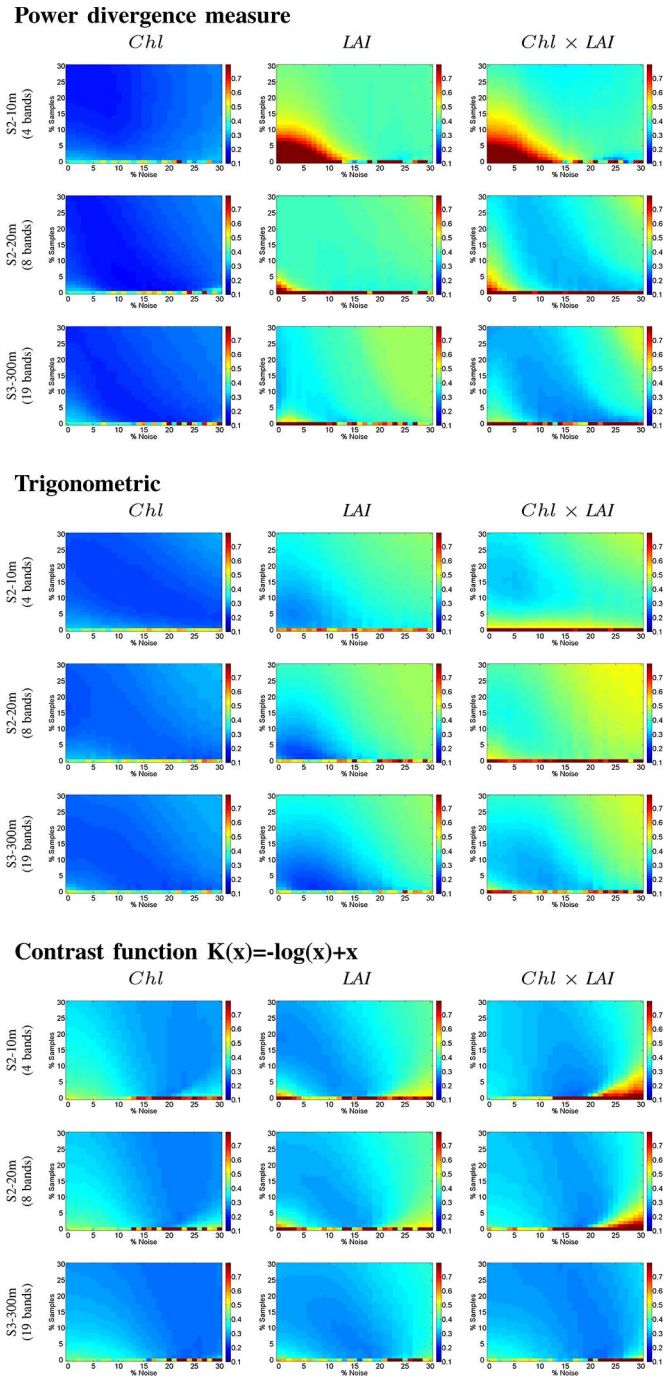

Fig. 2. RRMSE matrices (×100%) using "Power divergence measure" (top), "Trigonometric" (middle) and "Contrast function $K(x) = -\log(x) + x$" (bottom) as cost functions displaying the impact of % noise (X-axis) against multiple solutions (Y-axis) in LUT-based RTM inversion for S2-10 m, S2-20 m and S3-300 m data for leaf Chl, LAI and canopy Chl. The more bluish, the better the estimate.

Finally, the last tested cost function was "Contrast function $K(x) = -\log(x) + x$" [(4)]. Despite that this cost function performed about 5–7% poorer in retrieving leaf Chl than RMSE, it performed overall more stable than the other

TABLE IV
STATISTICS (r^2, RMSE, RRMSE) BASED ON BEST EVALUATED RRMSE AND CORRESPONDING MEAN MULTIPLE SOLUTIONS (%) AND NOISE LEVEL (%) USING "POWER DIVERGENCE MEASURE" (TOP), "TRIGONOMETRIC" (MIDDLE) AND "CONTRAST FUNCTION $K(x) = -\log(x) + x$" (BOTTOM) AS COST FUNCTIONS

Parameter	r^2	abs. RMSE	RRMSE	mult. sol. (%)	noise (%)
Power divergence measure					
S2-10m:					
Chl	0.71	7.86	19.38	23	6
LAI	0.62	0.93	28.84	0	15
$Chl \times$ LAI	0.86	34.32	23.15	0	27
S2-20m:					
Chl	0.75	7.52	18.38	2	16
LAI	0.66	1.11	36.84	1	18
$Chl \times$ LAI	0.74	39.14	29.71	1	23
S3-300m:					
Chl	0.75	8.43	19.86	1	15
LAI	0.67	0.90	30.52	0	27
$Chl \times$ LAI	0.76	34.92	26.28	1	17
Trigonometric					
S2-10m:					
Chl	0.60	8.87	22.15	10	14
LAI	0.71	0.82	27.25	5	3
$Chl \times$ LAI	0.66	41.10	31.52	15	5
S2-20m:					
Chl	0.58	8.90	23.07	17	0
LAI	0.82	0.66	22.27	1	6
$Chl \times$ LAI	0.61	44.99	37.10	14	4
S3-300m:					
Chl	0.64	9.06	22.36	1	19
LAI	0.80	0.68	21.23	1	7
$Chl \times$ LAI	0.70	39.11	31.33	4	10
Contrast function K(x)=-log(x)+x					
S2-10m:					
Chl	0.76	12.0	26.96	2	20
LAI	0.70	0.83	27.39	19	0
$Chl \times$ LAI	0.82	37.24	25.09	1	17
S2-20m:					
Chl	0.76	12.0	26.23	4	22
LAI	0.69	0.86	28.68	3	15
$Chl \times$ LAI	0.80	39.69	26.33	1	18
S3-300m:					
Chl	0.56	10.19	24.57	0	16
LAI	0.74	0.79	25.17	0	16
$Chl \times$ LAI	0.80	37.64	25.54	1	21

functions, with relative error results between 24–29% for all scenarios. As such, this function retrieved canopy Chl on the order of 15–25% better than RMSE. This function is formulated without additional parameters.

As we can see from the relative error matrices that different biophysical parameters provide different optimal distance which in mathematical terms proves the nonlinearity of the problem. The fact that each retrieved biophysical parameter identified a different optimal cost function shows that there is no linear correlation between these parameters and that the nature of error distribution is different and complicated. The fact that the accuracy of parameter estimation for tested functions changed with additional noise can also be explained. We added different levels of Gaussian noise to the already existing distribution of errors and therefore change the nature of distribution. Note that in general the sum of Gaussian with non-Gaussian errors gives non-Gaussian noise. Consequently, the change of error distribution leads us to different optimal cost functions. Overall, evaluated alternative cost functions can outperform the widely used RMSE, however, performances largely depend on the nature of the data, e.g., retrievable parameter, number of bands and regularization options.

TABLE V
STATISTICS (r^2, RMSE, RRMSE) BASED ON "CONTRAST FUNCTION$K(x) = -\log(x) + x$" AS COST FUNCTION WITH OPTIMIZED MULTIPLE SOLUTIONS (%) AND NOISE (%) PER SENTINEL CONFIGURATION

Parameter	r^2	abs. RMSE	RRMSE	mult. sol. (%)	noise (%)
Spectral					
S2-10m:					
Chl	0.76	14.57	29.75	1	17
LAI	0.71	0.89	29.92	1	17
$Chl \times$ LAI	0.83	37.24	25.09	1	17
S2-20m:					
Chl	0.77	14.01	28.52	1	18
LAI	0.69	0.93	30.82	1	18
$Chl \times$ LAI	0.80	39.69	26.33	1	18
S3-300m:					
Chl	0.73	13.22	27.49	1	20
LAI	0.70	0.86	27.89	1	20
$Chl \times$ LAI	0.81	39.27	25.93	1	20

C. Final Maps

In preparation to forthcoming S2 and S3 data streams, eventually the purpose of this work was to develop a LUT-based inversion strategy that enables concurrent mapping of multiple biophysical parameters. Hence, instead of repeating the computationally intensive inversion process with an optimized inversion strategy for each parameter, leaf Chl, LAI and canopy Chl were simultaneously retrieved using the cost function that performed most consistently over all three parameters. Spectral distance with "Contrast function $K(x) = -\log(x) + x$" would be most suitable for this task, not only because of being able retrieving parameters at the same degree of accuracy, but also because it is applicable without tuning additional parameters. Inspections of the relative error matrices show that a 1% multiple best solutions would be a good compromise to yield consistent results for all Sentinel configurations. Optimized noise levels slightly increased when having more bands included, with 17% noise for S2-10 m, 18% for S2-20 m and 20% for S3-300 m. As such, for each sentinel configuration leaf Chl, LAI and canopy Chl were simultaneously retrieved on a pixel-by-pixel basis. Validation statistics are provided in Table V. Despite that accuracies were slightly poorer than aforementioned individually optimized scenarios, they were consistent across all scenarios, with relative error accuracies between 25% and 31%. Final maps with mean estimations are shown in Fig. 3, and are briefly interpreted below.

To start with the most detailed S2-10 m map, pronounced within-field variations are notable by all three parameters. Particularly the spatial variation of canopy Chl clearly marks the irrigated circular fields with green biomass. These irrigated fields are characterized by a leaf Chl above 40 μg/cm^2 and LAI above 3. Areas with low $Chl(\leq 30$ μg/cm$^2)$ and LAI ($\leq$ 1.5) are mainly bare soils, fallow lands or senescent or harvested cereal fields (wheat, barley). It should herewith be noted that lower leaf Chl and to a lesser extent LAI estimates were expected over these dried-out lands (see also [51]), though no ground data were available to confirm these assumptions. The differences between green vegetation and dried-out vegetation are clearest observable in the canopy Chl maps. The somewhat coarser S2-20 m maps show essentially the same magnitudes of estimates and the same spatial patterns; within-field variability in the circular field are still clearly observable.

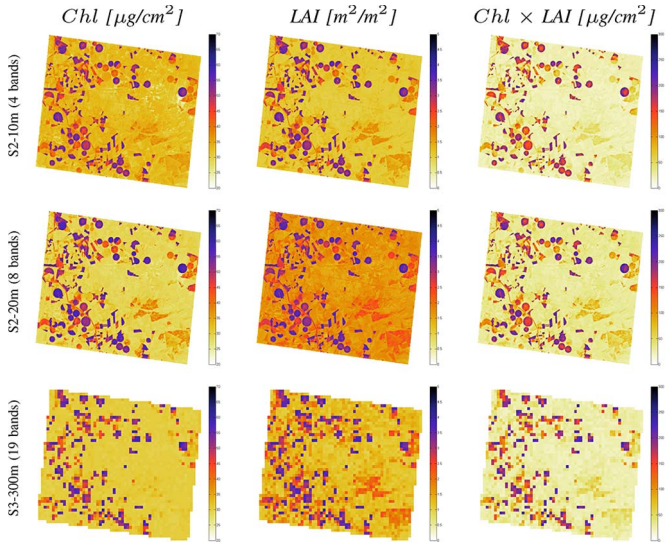

Fig. 3. Mean predictions of the 1% best solutions using "Contrast function $K(x) = -\log(x) + x$" as cost function in LUT-based RTM inversion ffor S2-10 m, S2-20 m and S3-300 m data for leaf Chl, LAI and canopy Chl.

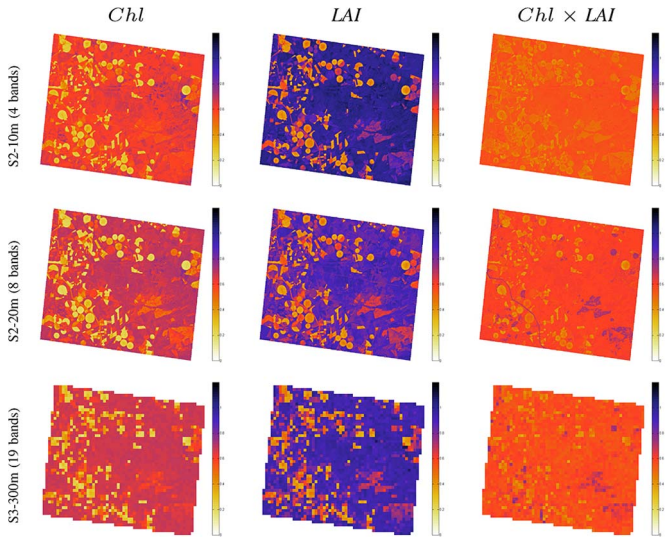

Fig. 4. Coefficient of variation (CV) of the 1% best solutions using "Contrast function $K(x) = -\log(x) + x$" as cost function in LUT-based RTM inversion for S2-10 m, S2-20 m and S3-300 m data for leaf Chl, LAI and canopy Chl.

Considerably coarser maps were obtained by the S3-300 m configuration. Although within-field spatial information has been mostly lost, spatial patterns of the irrigated fields are still notable.

Because the mean (μ) of the 1% best solutions was calculated, also the standard deviation [σ and coefficient of variation (CV; σ/μ) can be mapped. The latter is of interest as it allows comparison of the inversion performance across all maps (Fig. 4)]. Also, it is hard to interpret σ without μ, as higher mean estimates typically go along with higher σ. A relative indicator may therefore provide more information about the success of the retrieval, i.e., a lower CV means a greater uniformity across the 1% best solutions. The following observations can be made from these maps. First, consistent spatial patterns are obtained along the different Sentinel settings, which suggests that the number of bands did not play a major role in the inversion. Second, in each map lower CVs are realized over the vegetated parcels than over the dried-out lands. These areas are characterized by a low μ but a relatively high σ for the three biophysical parameters. This suggests that the generated LUT is better able to resolve the vegetated areas, which was to be expected since essentially variations in green canopy cover were simulated by PROSAIL. Third, LAI faced most difficulty in interpreting these dried-out lands. The encountered higher CV means that a larger variety of spectra and corresponding LAIs ended up in the top 1% best matching spectra. Conversely, the differences between the green and nongreen areas are smallest in the canopy Chl maps. This suggests that this combined parameter is having least difficulty in coping with surface heterogeneity encountered in the images. The underlying mechanism is that in the concurrent retrieval of multiple parameters the ill-posed problem appeared to be best resolved for canopy chl, probably at the expense of LAI. Overall, when inspecting both Figs. 3 and 4, it can be concluded that canopy Chl appeared to be a robust retrievable parameter over the whole imagery; it yielded realistic mean estimates while at the same time the CV maps suggested that the inversion problem was consistently resolved.

V. Discussion

A. Results in Comparison to Literature and Lessons Learned

Different optimization strategies have been evaluated in this work. Best obtained inversion results were on the order of 18% for leaf Chl, 21% for LAI and 23% for canopy Chl. It should however be noted that neither the 10% threshold required by GMES nor the order of accuracies as encountered in likewise studies using the SPARC data set were reached. For instance, [37] reached LAI accuracies around 10% for specific crops such as sugar beet and wheat, while maize accuracies were around 19%. Also, [40] achieved better accuracies with the same data set for specific crop types through spatially constrained inversion but failed for row-planted crops as maize, potatoes and sunflowers. Nevertheless, all these approaches assumed that spatial information of the vegetation types is available, so that inversion can take place at the scale of a single agricultural field. In part, this suggests that the reported successful results were rather due to the intrinsic characteristics of the land cover type (e.g., more homogeneous) than to the proposed retrieval approach. This is an important point to address, since agroecosystems are generally patchy, meaning that acquired imageries span a multitude of land cover types, both structurally homogeneous and heterogeneous. In view of forthcoming Sentinel data streams it cannot be expected that up-to-date land cover information at the high spatial resolution of S2, i.e., at 10 m, is instantaneously available. Further, beyond agroecosystems, the spatially constrained inversion approaches proposed in [37], [40], and [41] would not be possible to apply over more natural vegetated areas, which are structurally more heterogeneous and lack clearly defined boundaries. Retrieval performances should therefore merely be evaluated over a variety of crop types without constraining the inversion to specific

parcels. Another point is that all aforementioned LUT-based inversion studies used RMSE as cost function. We found that the commonly used RMSE distance is not the optimal cost function for the cases studied and that better results can be obtained using alternative statistical distances. This could be explained by nonlinearities and robustness of the problem and also by non-Gaussian and skewed noise.

Regardless of having spatial information available, a successful strategy for concurrent mapping of multiple biophysical parameters over large areas may be through the use regularization strategies and alternative cost functions. We used a generic LUT without assuming any on-site spatial knowledge for pixel-based inversion over complete simulated Sentinel-2 and -3 imageries. From a list of more than 60 cost functions we have evaluated three promising functions with respect to multiple bands, noise and multiple best solutions in LUT-based inversion. Several conclusions can be drawn from this study, which can function as guidelines for future retrieval strategies.

Role of Alternative Cost Functions: Three different classes of cost functions were used, where one representative from each class was selected to provide the alternative to the RMSE. It was found that for all scenarios (parameters and Sentinel settings) one or more of the tested cost functions outperformed RMSE in LUT-based inversion. It was however not the case that substantial improvements were achieved by one single cost function over all scenarios. This proves the nonlinearity of the problem and can be explained by the different parameters dealing with different types of error distributions. That RMSE did not perform very well over LAI and canopy Chl means that the correspondent distribution for these estimated parameters is non-Gaussian. Application of alternative cost functions can interpret the error distribution more accurately and provide better results. The "Power divergence measure" outperformed RMSE in every single scenario but this function yielded only a small improvement for leaf Chl and was not best evaluated function for LAI and canopy Chl retrieval. It should also be noted that this measure was performing similarly as other divergence measures described in [39] such as "Rènyi", "Sharma-Mittal" and "Cressie and Read (1984)" (results not shown). The drawback of these functions is that they require some fine-tuning of their parameter which demand for further testing of the optimal problem. A follow-up study will be devoted to systematically assessing its role in the inversion process. The cost function "Trigonometric" performed more stable over LAI and canopy Chl but it requires two parameters to be tuned. It led to robust LAI retrievals with in case of S3-300 m a best relative error of 21.2%. Such a good accuracy was not achieved when using "Contrast function $K(x) = -\log(x) + x$" distance, but this function obtained robust estimates for canopy Chl and yielded most consistent retrievals over all parameters, with best accuracies between 24.6% and 28.7%. Overall, it was found that leaf Chl was best retrieved by "Power divergence measure" (up to 2% better than RMSE), LAI by "Trigonometric" (up to 9% better than RMSE) and canopy Chl by spectral distance with "Contrast function $K(x) = -\log(x) + x$" (up to 15% better than RMSE). This leads us concluding that the RMSE does not always behave as an optimal cost function in LUT-based inversion.

Role of Regularization Options: The introduction of added noise and multiple solutions in the inversion process led to considerable improvements as compared to the cases without using them. Its impact, however, strongly depended on the considered parameter and cost function. For instance, when using RMSE or "Power divergence measure", variations in regularization options hardly impacted leaf Chl retrieval until high noise levels were reached (e.g., $> 20\%$). In turn, these regularizations substantially impacted the performance of LAI and canopy Chl. Although its absence or even low levels led to poor retrievals, injecting quite some noise (e.g., 15–25%) in combination to multiple best solutions ($\geq 1\%$) greatly improved retrievals, with best relative error results between 28.8% and 40.4%. Because results were on the whole better for "Trigonometric" and "Contrast function $K(x) = -\log(x) + x$" the impact of regularization options was less pronounced. Yet, clear patterns within each relative error matrix demonstrate that also these functions gained from regularizations options.

Role of Number of Bands: The number of bands had some effect on retrieval performances but not for all parameters and cost functions. For instance, for each of the cost functions similar leaf Chl results were obtained in the relative error matrices across the different Sentinel band settings. This suggests that already good leaf Chl retrievals were achieved at the configuration of S2-10 m (four bands), while adding bands did not much enhance the inversion. Its underlying mechanism can be explained by the fact that in PROSAIL variation in leaf Chl only impacts the visible range, e.g., at 665 nm where maximal absorption takes place, right where the S2-10 m bands B2, B3 and B4 are located. LAI and canopy Chl gained more from added bands, as can be clearly observed across RMSE and "Power divergence measure" matrices where regions with failure diminished when moving to S2-20 m and S3-300 m. The reason for some improvements is that LAI is impacted by the whole visible and NIR range, including red-edge thus added bands can help improving the inversion [64]. For the two other cost functions this trend was less pronounced; good results were already obtained at S2-10 m when using regularization options. The good performance of the cost function with "Contrast function $K(x) = -\log(x) + x$" across the different Sentinel configurations became also clear when inspecting the final maps; differences in the spatial patterns appeared to be minimal.

Role of Combined Variables: Despite encouraging suggestions in similar studies [25], [29], [33], [38], for the majority of tested cost functions did the combined Chl x LAI (canopy Chl) not lead to significant improvements. Only in case of S2-10 m when "Contrast function $K(x) = -\log(x) + x$" was used then canopy Chl slightly outperformed leaf Chl and LAI. When inspecting the final CV maps, however, it can be observed that canopy Chl obtained generally lower values than the other parameters, meaning that the 1% best spectra wherefrom the mean estimate is calculated, were more uniform and thus narrowing the ill-posed problem. This difference was particularly notable over the non-irrigated dry lands. Given this all, canopy Chl proved its use as a robust retrievable parameter and deserves to be included in the package of deliverable products.

B. Towards Robust Operational LUT-BASED Retrievals From S2 and S3 Imagery

Despite claims from case studies [24], [37], [40] that LUT-based RTM inversion can be a successful approach for operational delivering of biophysical products from Sentinel data streams, based on here presented results we can only partly agree. Although being physically based and therefore more universally applicable, LUT-based RTM inversion in its essential form, i.e., through the use of cost functions, can only be successful in an operational context when performances are robust over the complete image, i.e., spanning multiple land cover types. We have exploited this concept to the fullest by simulating S2 and S3 images, but accuracies did not reach the desired threshold of 10%.

In comparison, in a parallel study the same experimental data set (field measurements and corresponding spectra for the various Sentinel settings) was fed into advanced machine learning regression algorithms (MLRAs) [51]. In these approaches regression models are trained from the experimental data itself. An advantage of MLRAs is that interpretation of an image occurs almost instantaneously once having a model trained. This in contrast to the LUT-based inversion approach, which requires pixel-by-pixel processing against the complete LUT, and is therefore more computationally demanding. MLRAs yielded excellent results over the whole image, e.g., the best evaluated method, Gaussian processes regression, yielded relative error results for S2-20 m and S3-300 m on the order of 23% for LAI and 7% for leaf Chl. While here similar LAI accuracies were obtained when using "Trigonometric" as cost function, a considerable gap remains to be bridged with respect to leaf Chl. One explanation may be that the generated LUT was insufficiently large, although according to [38] this impact should be small. A more relevant explanation may be that RTMs are often unable to mimic properly actual TOC spectral observations. Consequently, due to model uncertainties and simplifications large variations may be induced in the solution of the inverse problem [33]. It remains however to be investigated how robust these MLRAs would perform when applied to imagery that deviates from the local training data set, as is typically the case in an operational context. The lack of universality is a well-known limitation of statistically based methods compared to physically based methods. To make these MLRAs more generic, they should be learned by a broad range of spectra that is sufficiently able to mimic spectral observations as acquired by any imagery. A promising avenue for further investigation is to implement these MLRAs into ARTMO so that they can be trained by a massive amount of simulated spectra, e.g., such as the here generated LUT.

Finally, another promising avenue to be investigated, assuming that no up-to-date land cover map at the scale of 10 m is available, is relying on vegetation indices to spatially constrain the LUTs. For instance, vegetation indices are able to detect bare soil, water bodies, sparsely vegetated areas and densely vegetated areas (e.g., see also [35]). This information could then function to constrain LUTs on a per-pixel basis. Also, this approach is currently explored to be implemented in ARTMO.

VI. Conclusion

ESA's forthcoming Sentinel-2 (S2) and Sentinel-3 (S3) satellites aim to improve the old generation of satellite sensors through enhanced sensor configurations. At the same time, there is also a need for improved retrieval methods of biophysical parameters such as leaf Chl, LAI and canopy Chl. While various LUT-based inversion methods have been proposed in literature they all rely on RMSE as cost function. However, RMSE can result in large losses of efficiency when the error distribution is non-Gaussian or nonsymmetric. For the benefit of realizing improved retrievals, we have compared three alternative cost functions ("Power divergence measure", Trigonometric' and "Contrast function $K(x) = -\log(x) + x$") using S2 and S3 data sets, i.e., S2 at 10 m (4 bands), 20 m (8 bands) and S3-OLCI at 300 m (19 bands). These cost functions outperformed the widely used RMSE, although this also depended on the retrievable parameter, since they all have different nature of error distribution. Introducing noise and applying multiple best solutions in the inversion further improved the inversion performance. Overall, leaf Chl was best retrieved by "Power divergence measure", LAI by "Trigonometric" distance and canopy Chl by spectral distance with the "Contrast function $K(x) = -\log(x) + x$". The latter was also evaluated as best suited for simultaneous retrieval of these biophysical parameters. Maps were obtained and showed consistent performances across the Sentinel configurations, which suggests that the here tested parameters can be routinely mapped by S2 already at a high spatial resolution of 10 m. Summarizing, for 3 different Sentinel settings (S2-10 m, S2-20 m, S3-300 m) it has been demonstrated that the success of LUT-based inversion strongly depends on the retrievable parameter and applied regularization options. Their performance is directly related to the used cost function due to different assumptions on the nature and properties of errors. It is therefore recommended to evaluate different inversion strategies prior to applying an inversion strategy to the whole image.

Acknowledgment

The authors would like to thank the three anonymous reviewers for their valuable comments.

References

[1] R. H. Whittaker and P. L. Marks, "Methods of assessing terrestrial productivity," in *Primary Productivity of the Biosphere*. New York, NY, USA: Springer-Verlag, 1975, pp. 55–118.

[2] H. K. Lichtenthaler, "Chlorophylls and carotenoids: Pigments of photosynthetic biomembranes," *Methods Enzymol.*, vol. 148, pp. 350–382, 1987.

[3] H. K. Lichtenthaler, M. Lang, M. Sowinska, F. Heisel, and J. A. Miehe, "Detection of vegetation stress via a new high resolution fluorescence imaging system," *J. Plant Physiol.*, vol. 148, no. 5, pp. 599–612, 1996.

[4] P. H. Sampson, P. J. Zarco-Tejada, G. H. Mohammed, J. R. Miller, and T. L. Noland, "Hyperspectral remote sensing of forest condition: Estimating chlorophyll content in tolerant hardwoods," *Forest Sci.*, vol. 49, no. 3, pp. 381–391, 2003.

[5] A. A. Gitelson, A. Vina, S. B. Verma, D. C. Rundquist, T. J. Arkebauer, G. Keydan, B. Leavitt, V. Ciganda, G. G. Burba, and A. E. Suyker, "Relationship between gross primary production and chlorophyll content in crops: Implications for the synoptic monitoring of vegetation productivity," *J. Geophys. Res. D, Atmosp.*, vol. 111, no. D8, pp. D08S11-1–D08S11-13, Apr. 2006.

[6] T. Hirose, D. D. Ackerly, M. B. Traw, D. Ramseier, and F. A. Bazzaz, "CO2 elevation, canopy photosynthesis, and optimal leaf area index," *Ecology*, vol. 78, no. 8, pp. 2339–2350, 1997.

[7] F. Baret and G. Guyot, "Potentials and limits of vegetation indices for LAI and APAR assessment," *Remote Sens. Environ.*, vol. 35, no. 2/3, pp. 161–173, Feb./Mar. 1991.

[8] P. Bicheron and M. Leroy, "A method of biophysical parameter retrieval at global scale by inversion of a vegetation reflectance model," *Remote Sens. Environ.*, vol. 67, no. 3, pp. 251–266, Mar. 1999.

[9] W. Buermann, J. Dong, X. Zeng, R. B. Myneni, and R. E. Dickinson, "Evaluation of the utility of satellite-based vegetation leaf area index data for climate simulations," *J. Climate*, vol. 14, no. 17, pp. 3536–3550, Sep. 2001.

[10] V. G. Kakani, K. R. Reddy, D. Zhao, and K. Sailaja, "Field crop responses to ultraviolet-B radiation: A review," *Agric. Forest Meteorol.*, vol. 120, no. 1–4, pp. 191–218, Dec. 2003.

[11] J. Aschbacher and M. P. Milagro-Pérez, "The European earth monitoring GMES programme: Status and perspectives," *Remote Sens. Environ.*, vol. 120, pp. 3–8, May 2012.

[12] M. Berger, J. Moreno, J. A. Johannessen, P. F. Levelt, and R. F. Hanssen, "ESA's sentinel missions in support of Earth system science," *Remote Sens. Environ.*, vol. 120, pp. 84–90, May 2012.

[13] N. Gobron, "Theoretical limits to the estimation of the leaf area index on the basis of visible and near-infrared remote sensing data," *IEEE Trans. Geosci. Remote Sens.*, vol. 35, no. 6, pp. 1438–1445, Nov. 1997.

[14] J. Verrelst, M. E. Schaepman, B. Koetz, and M. Kneubühler, "Angular sensitivity analysis of vegetation indices derived from CHRIS/PROBA data," *Remote Sens. Environ.*, vol. 112, no. 5, pp. 2341–2353, May 2008.

[15] J. Verrelst, M. E. Schaepman, Z. Malenovský, and J. G. P. W. Clevers, "Effects of woody elements on simulated canopy reflectance: Implications for forest chlorophyll content retrieval," *Remote Sens. Environ.*, vol. 114, no. 3, pp. 647–656, Mar. 2010.

[16] J. Ross, *The Radiation Regime and Architecture of Plant Stands*. The Hague, The Netherlands: Dr. W. Junk. Publ., 1981, pt. 391 pp.

[17] S. Jacquemoud, W. Verhoef, F. Baret, C. Bacour, P. J. Zarco-Tejada, G. P. Asner, C. François, and S. L. Ustin, "PROSPECT + SAIL models: A review of use for vegetation characterization," *Remote Sens. Environ.*, vol. 113, no. Suppl. 1, pp. S56–S66, Sep. 2009.

[18] W. A. Dorigo, R. Zurita-Milla, A. J. W. de Wit, J. Brazile, R. Singh, and M. E. Schaepman, "A review on reflective remote sensing and data assimilation techniques for enhanced agroecosystem modeling," *Int. J. Appl. Earth Observ. Geoinf.*, vol. 9, no. 2, pp. 165–193, May 2007.

[19] R. Darvishzadeh, A. Skidmore, M. Schlerf, and C. Atzberger, "Inversion of a radiative transfer model for estimating vegetation lai and chlorophyll in a heterogeneous grassland," *Remote Sens. Environ.*, vol. 112, no. 5, pp. 2592–2604, May 2008.

[20] Y. Knyazikhin, J. Kranigk, R. B. Myneni, O. Panfyorov, and G. Gravenhorst, "Influence of small-scale structure on radiative transfer and photosynthesis in vegetation canopies," *J. Geophys. Res. D, Atmosp.*, vol. 103, no. D6, pp. 6133–6144, Jan. 1998.

[21] S. S. Durbha, R. L. King, and N. H. Younan, "Support vector machines regression for retrieval of leaf area index from multiangle imaging spectroradiometer," *Remote Sens. Environ.*, vol. 107, no. 1/2, pp. 348–361, Mar. 2007.

[22] W. A. Dorigo, "Improving the robustness of cotton status characterisation by radiative transfer model inversion of multi-angular CHRIS/PROBA data," *IEEE J. Sel. Topics Applied Earth Observ. Remote Sens.*, vol. 5, no. 1, pp. 18–29, Feb. 2012.

[23] B. Combal, F. Baret, M. Weiss, A. Trubuil, D. Mac, A. Pragnère, R. Myneni, Y. Knyazikhin, and L. Wang, "Retrieval of canopy biophysical variables from bidirectional reflectance using prior information to solve the ill-posed inverse problem," *Remote Sens. Environ.*, vol. 84, no. 1, pp. 1–15, Jan. 2003.

[24] K. Richter, C. Atzberger, F. Vuolo, P. Weihs, and G. D'Urso, "Experimental assessment of the sentinel-2 band setting for RTM-based LAI retrieval of sugar beet and maize," *Can. J. Remote Sens.*, vol. 35, no. 3, pp. 230–247, 2009.

[25] M. Weiss, F. Baret, R. B. Myneni, A. Pragnère, and Y. Knyazikhin, "Investigation of a model inversion technique to estimate canopy biophysical variables from spectral and directional reflectance data," *Agronomie*, vol. 20, no. 1, pp. 3–22, Jan./Feb. 2000.

[26] M. Vohland, S. Mader, and W. Dorigo, "Applying different inversion techniques to retrieve stand variables of summer barley with PROSPECT + SAIL," *Int. J. Appl. Earth Observ. Geoinf.*, vol. 12, no. 2, pp. 71–80, Apr. 2010.

[27] H. Fang and S. Liang, "A hybrid inversion method for mapping leaf area index from MODIS data: Experiments and application to broadleaf and needleleaf canopies," *Remote Sens. Environ.*, vol. 94, no. 3, pp. 405–424, Feb. 2005.

[28] C. Walthall, W. Dulaney, M. Anderson, J. Norman, H. Fang, and S. Liang, "A comparison of empirical and neural network approaches for estimating corn and soybean leaf area index from landsat ETM+ imagery," *Remote Sens. Environ.*, vol. 92, no. 4, pp. 465–474, Sep. 2004.

[29] C. Bacour, F. Baret, D. Béal, M. Weiss, and K. Pavageau, "Neural network estimation of LAI, fAPAR, fCover and LAI $\times$ Cab, from top of canopy MERIS reflectance data: Principles and validation," *Remote Sens. Environ.*, vol. 105, no. 4, pp. 313–325, Dec. 2006.

[30] M. Weiss and F. Baret, "Evaluation of canopy biophysical variable retrieval performances from the accumulation of large swath satellite data," *Remote Sens. Environ.*, vol. 70, no. 3, pp. 293–306, Dec. 1999.

[31] Y. Qu, J. Wang, H. Wan, X. Li, and G. Zhou, "A Bayesian network algorithm for retrieving the characterization of land surface vegetation," *Remote Sens. Environ.*, vol. 112, no. 3, pp. 613–622, Mar. 2008.

[32] S. Jacquemoud, F. Baret, B. Andrieu, F. M. Danson, and K. Jaggard, "Extraction of vegetation biophysical parameters by inversion of the PROSPECT+SAIL models on sugar beet canopy reflectance data. application to TM and AVIRIS sensors," *Remote Sens. Environ.*, vol. 52, no. 3, pp. 163–172, Jun. 1995.

[33] B. Combal, F. Baret, and M. Weiss, "Improving canopy variables estimation from remote sensing data by exploiting ancillary information. Case study on sugar beet canopies," *Agronomie*, vol. 22, no. 2, pp. 205–215, Mar. 2002.

[34] F. Baret and S. Buis, "Estimating canopy characteristics from remote sensing observations. Review of methods and associated problems," in *Advances in Land Remote Sensing: System, Modeling, Inversion, and Application*. New York, NY, USA: Springer-Verlag, 2008.

[35] W. Dorigo, R. Richter, F. Baret, R. Bamler, and W. Wagner, "Enhanced automated canopy characterization from hyperspectral data by a novel two step radiative transfer model inversion approach," *Remote Sens.*, vol. 1, no. 4, pp. 1139–1170, Nov. 2009.

[36] B. Koetz, F. Baret, H. Poilvé, and J. Hill, "Use of coupled canopy structure dynamic and radiative transfer models to estimate biophysical canopy characteristics," *Remote Sens. Environ.*, vol. 95, no. 1, pp. 115–124, Mar. 2005.

[37] K. Richter, C. Atzberger, F. Vuolo, and G. D'Urso, "Evaluation of sentinel-2 spectral sampling for radiative transfer model based LAI estimation of wheat, sugar beet, and maize," *IEEE J. Sel. Topics Appl. Earth Observ. Remote Sens.*, vol. 4, no. 2, pp. 458–464, Jun. 2011.

[38] R. Darvishzadeh, A. A. Matkan, and A. Dashti Ahangar, "Inversion of a radiative transfer model for estimation of rice canopy chlorophyll content using a lookup-table approach," *IEEE J. Sel. Topics Appl. Earth Observ. Remote Sens.*, vol. 5, no. 4, pp. 1222–1230, Aug. 2012.

[39] G. Leonenko, P. R. J. North, and S. O. Los, "Statistical distances and their applications to biophysical parameter estimation. Information measures, m-estimates, minimum contrast method," *Remote Sens.*, 2013, submitted for publication.

[40] C. Atzberger and K. Richter, "Spatially constrained inversion of radiative transfer models for improved LAI mapping from future sentinel-2 imagery," *Remote Sens. Environ.*, vol. 120, pp. 208–218, May 2012.

[41] R. Houborg, M. Anderson, and C. Daughtry, "Utility of an image-based canopy reflectance modeling tool for remote estimation of lai and leaf chlorophyll content at the field scale," *Remote Sens. Environ.*, vol. 113, no. 1, pp. 259–274, Jan. 2009.

[42] J. Verrelst, J. P. Rivera, L. Alonso, and J. Moreno, "ARTMO: An Automated radiative transfer models operator toolbox for automated retrieval of biophysical parameters through model inversion," in *Proc. EARSeL 7th SIG-Imag. Spectrosc. Workshop*, Edinburgh, U.K., 2011.

[43] J. Verrelst, E. Romijn, and L. Kooistra, "Mapping vegetation density in a heterogeneous river floodplain ecosystem using pointable CHRIS/PROBA data," *Remote Sens.*, vol. 4, no. 9, pp. 2866–2889, Sep. 2012.

[44] L. Pardo, *Statistical Inference Based on Divergence Measures (Statistics: A Series Textbooks and Monographs)*. London, U.K.: Chapman & Hall, 2006.

[45] B. G. Lindsay, "Efficiency versus robustness: The case for minimum hellinger distance and related methods," *Ann. Stat.*, vol. 22, no. 2, pp. 1081–1114, 1994.

[46] R. G. Staudte and S. J. Sheather, *Robust Estimation and Testing*. New York, NY, USA: Wiley, 1990.

[47] M. Taniguchi, "On estimation of parameters of Gaussian stationary processes," *J. Appl. Probab.*, vol. 16, no. 3, pp. 575–591, Sep. 1979.

[48] M. Taniguchi, "Minimum contrast estimation for spectral densities of stationary processes," *J. Roy. Stat. Soc.: Ser. B (Stat. Methodol.)*, vol. 49, no. 3, pp. 315–325, 1987.

[49] S. Gandía, G. Fernández, J. C. Garcia, and J. Moreno, "Retrieval of vegetation biophysical variables from CHRIS/PROBA data in the SPARC campaign," in *Proc. 2nd CHRIS/PROBAWorkshop*, Frascati, Italy, 2004.

[50] G. Fernández, J. Moreno, S. Gandía, B. Martínez, F. Vuolo, and F. Morales, "Statistical variability of field measurements of biophysical parameters in SPARC-2003 and SPARC-2004 campaigns," in *Proc. SPARC Workshop*, 2005, CD-ROM.

[51] J. Verrelst, J. Munoz, L. Alonso, J. Delegido, J. P. Rivera, G. Camps-Valls, and J. Moreno, "Machine learning regression algorithms for biophysical parameter retrieval: Opportunities for Sentinel-2 and -3," *Remote Sens. Environ.*, vol. 118, pp. 127–139, Mar. 2012.

[52] J. Verrelst, L. Alonso, G. Camps-Valls, J. Delegido, and J. Moreno, "Retrieval of vegetation biophysical parameters using Gaussian process techniques," *IEEE Trans. Geosci. Remote Sens.*, vol. 50, no. 5, pp. 1832–1843, May 2012.

[53] J. Delegido, G. Fernandez, S. Gandía, and J. Moreno, "Retrieval of chlorophyll content and LAI of crops using hyperspectral techniques: Application to PROBA/CHRIS data," *Int. J. Remote Sens.*, vol. 29, no. 24, pp. 7107–7127, Dec. 2008.

[54] J. Delegido, L. Alonso, G. González, and J. Moreno, "Estimating chlorophyll content of crops from hyperspectral data using a normalized area over reflectance curve (NAOC)," *Int. J. Appl. Earth Observ. Geoinf.*, vol. 12, no. 3, pp. 165–174, Jun. 2010.

[55] M. Drusch, U. Del Bello, S. Carlier, O. Colin, V. Fernandez, F. Gascon, B. Hoersch, C. Isola, P. Laberinti, P. Martimort, A. Meygret, F. Spoto, O. Sy, F. Marchese, and P. Bargellini, "Sentinel-2: ESA's optical high-resolution mission for GMES operational services," *Remote Sens. Environ.*, vol. 120, pp. 25–36, May 2012.

[56] M. Drusch, F. Gascon, and M. Berger, Sentinel-2 Mission Requirements Document 2010. [Online]. Available: http://esamultimedia.esa.int/docs/GMES/Sentinel-2_MRD.pdf

[57] C. Donlon, B. Berruti, A. Buongiorno, M.-H. Ferreira, P. Féménias, J. Frerick, P. Goryl, U. Klein, H. Laur, C. Mavrocordatos, J. Nieke, H. Rebhan, B. Seitz, J. Stroede, and R. Sciarra, "The global monitoring for environment and security GMES sentinel-3 mission," *Remote Sens. Environ.*, vol. 120, pp. 37–57, May 2012.

[58] M. J. Barnsley, J. J. Settle, M. A. Cutter, D. R. Lobb, and F. Teston, "The PROBA/CHRIS mission: A low-cost smallsat for hyperspectral multiangle observations of the earth surface and atmosphere," *IEEE Trans. Geosci. Remote Sens.*, vol. 42, no. 7, pp. 1512–1520, Jul. 2004.

[59] L. Alonso and J. Moreno, "Advances and limitations in a parametric geometric correction of CHRIS/PROBA data," in *Proc. 3rd CHRIS/Proba Workshop*, Frascati, Italy, 2005.

[60] L. Guanter, L. Alonso, and J. Moreno, "A method for the surface reflectance retrieval from PROBA/CHRIS data over land: Application to ESA SPARC campaigns," *IEEE Trans. Geosci. Remote Sens.*, vol. 43, no. 12, pp. 2908–2917, Dec. 2005.

[61] J. B. Feret, C. François, G. P. Asner, A. A. Gitelson, R. E. Martin, L. P. R. Bidel, S. L. Ustin, G. le Maire, and S. Jacquemoud, "PROSPECT-4 and 5: Advances in the leaf optical properties model separating photosynthetic pigments," *Remote Sens. Environ.*, vol. 112, no. 6, pp. 3030–3043, Jun. 2008.

[62] W. Verhoef, L. Jia, Q. Xiao, and Z. Su, "Unified optical-thermal four-stream radiative transfer theory for homogeneous vegetation canopies," *IEEE Trans. Geosci. Remote Sens.*, vol. 45, no. 6, pp. 1808–1822, Jun. 2007.

[63] F. Baret, O. Hagolle, B. Geiger, P. Bicheron, B. Miras, M. Huc, B. Berthelot, F. Niço, M. Weiss, O. Samain, J. L. Roujean, and M. Leroy, "LAI, fAPAR and fcover CYCLOPES global products derived from VEGETATION. Part 1: Principles of the algorithm," *Remote Sens. Environ.*, vol. 110, no. 3, pp. 275–286, Oct. 2007.

[64] J. Delegido, J. Verrelst, L. Alonso, and J. Moreno, "Evaluation of sentinel-2 red-edge bands for empirical estimation of green LAI and chlorophyll content," *Sensors*, vol. 11, no. 7, pp. 7063–7081, Jul. 2011.

Jochem Verrelst received the M.Sc. degree in tropical land use and in geo-information science both in 2005 and the Ph.D. in remote sensing in 2010 from Wageningen University, Wageningen, Netherlands. His dissertation focused on the space-borne spectrodirectional estimation of forest properties.

Since March 2010, he has been a Marie Curie Postdoctoral Fellow at the Laboratory for Earth Observation, Image Processing Laboratory, University of Valencia, University of Valencia, Spain. Currently, he is involved in preparatory activities of the Fluorescence Explorer. His research interests include retrieval of vegetation properties using airborne and satellite data, canopy radiative transfer modeling, and multiangular and hyperspectral data analysis.

Juan Pablo Rivera received the B.Sc. degree in agricultural engineering from the University National of Colombia, Bogotá, Columbia and Univerity of Valle, Cali, Colombia, in 2001, the Master degree in irrigation engineering from the CEDEX-Centro de Estudios y Experimentación de Obras Publicas-, El Goloso, Spain, in 2003, and the M.Sc. degree in Remote sensing from the University of Valencia, Valencia, Spain.

Since January 2011, he has been a member of the Laboratory for Earth Observation, Image Processing Laboratory, University of Valencia, Spain as a Ph.D. candidate. Currently, he is involved in preparatory activities of the Fluorescence Explorer. His research interests include retrieval of vegetation properties using airborne and satellite data, leaf and canopy radiative transfer modeling and hyperspectral data analysis.

Ganna Leonenko received the diploma degree in mathematics and the M.S. degree in statistics from Kyiv T. Shevchenko University, Kiev, Ukraine, in 2001 and in 2002, respectively, and the Ph.D. degree in operation research and statistics from Cardiff University, Wales, U.K., in 2006.

From 2005 to 2008, she was a Reasearch Associate in non-Newtonian fluid dynamics, Cardiff University, studying multi-dimensional Fokker-Planck equation. She became a research officer in remote sensing group in Swansea University, Swansea University, U.K. (2008–2012) where she worked in a field of statistical methods in biophysical parameter retieval using remotely sensed data. Currently, she works in statistical genetics and bioinformatics in application to mental diseases at Cardiff University. Her research areas also involve financial mathematics, diffusion processes, queueing systems, and spectral numerical methods.

Luis Alonso received the B.Sc. degree in physics and the M.S. degree in environmental physics from the University of Valencia, Valencia, Spain, in 1999 and 2002, respectively, while working on the geometric correction of airborne and spaceborne remote sensing imagery.

He is member of the Laboratory for Earth Observation at the Image Processing Laboratory of the University of Valencia, where he studies the remote sensing of chlorophyll fluorescence at canopy level. He has participated in several preparatory studies for FLEX candidate mission for ESA's Earth Explorers as well as for GMES Sentinel-2 and Sentinel-3.

José Moreno (A'89–M'09) received the M.Sc. degree in physics and the Ph.D. degree in theoretical physics from the University of Valencia, Valencia, Spain, in 1992.

He is currently at the Department of Earth Physics and Thermodynamics, Faculty of Physics of the University of Valencia, as Professor of Earth Physics, teaching and working on different projects related to remote sensing and space research as responsible for the Laboratory for Earth Observation. His main work is related to the modeling and monitoring of land surface processes by using remote sensing techniques. He has been involved in many international projects and research networks. He has been involved in the preparatory activities an exploitation programmes of several satellite missions (ENVISAT, CHRIS/PROBA, GMES/Sentinels, SEOSAT) and the Fluorescence Explorer, a candidate ESA Earth Explorer Core Mission.

Dr. Moreno has served as Associate Editor for the IEEE TRANSACTIONS ON GEOSCIENCE AND REMOTE SENSING (1994–2000) and has been a member of the ESA Earth Sciences Advisory Committee (1998–2002), the Space Station Users Panel, and other international advisory committees. He is Director of the Laboratory for Earth Observation (LEO) at the Image Processing Laboratory/Scientific Park.